

Cluster formation and phase separation in heteronuclear Janus dumbbells

G Munaò^{1‡}, P O'Toole², T S Hudson², D Costa¹,
C Caccamo¹, F Sciortino³ and A Giacometti⁴

¹Dipartimento di Fisica e di Scienze della Terra, Università degli Studi di Messina,
Viale F. Stagno d'Alcontres 31, 98166 Messina, Italy

²School of Chemistry, University of Sidney, NSW 2006, Australia

³Dipartimento di Fisica, Università di Roma "Sapienza", Piazzale Aldo Moro 2,
00185 Roma, Italy

⁴Dipartimento di Scienze Molecolari e Nanosistemi, Università Ca' Foscari Venezia,
Calle Larga S. Marta DD2137, Venezia I-30123, Italy

Abstract. We have recently investigated the phase behaviour of model colloidal dumbbells constituted by two identical tangent hard spheres, with the first one being surrounded by an attractive square-well interaction (Janus dumbbells, Munaó G *et al* 2014 *Soft Matter* **10** 5269). Here we extend our previous analysis by introducing in the model the size asymmetry of the hard-core diameters, and study the enriched phase scenario thereby obtained. By employing standard Monte Carlo simulations we show that in such "heteronuclear Janus dumbbells" a larger hard-sphere site promotes the formation of clusters, whereas in the opposite condition a gas-liquid phase separation takes place, with a narrow interval of intermediate asymmetries wherein the two phase behaviours may compete. In addition, some peculiar geometrical arrangements, such as lamellæ, are observed only around the perfectly symmetric case. A qualitative agreement is found with recent experimental results, where it is shown that the roughness of molecular surfaces in heterogeneous dimers leads to the formation of colloidal micelles.

1. Introduction

Colloidal dumbbells are currently object of rather intense experimental [1–7] and theoretical investigations [8–10], due to the possibility offered by such particles to act as building blocks for the fabrication of new materials [4], such as photonic crystals [5], self-assembled structures under the effect of electric fields [6] and other complex structures [7]. One key feature of such dumbbells is the asymmetry in the relative size of the constituting spheres and/or in their interaction potential. Pure hard-sphere, as well as pure square-well colloidal dumbbells have been widely studied, with a variety of investigation concerning their thermodynamic and structural properties [11–21]. In the special case in which one of the two particles is solvophilic, and the other

‡ Corresponding author: gmunao@unime.it

one is solvophobic, the “molecule” represents a simple example of a colloidal surfactant (Janus dumbbell [22, 23]). Such systems constitute a molecular generalization of the well-known concept of Janus spherical particles [24–30], largely investigated because of the rich variety of self-assembled structures they may form. In the Janus dumbbell case, such a scenario may be further enriched by the possibility to tune the aspect ratio and the asymmetry of the dumbbell, thus originating what we shall henceforth term heteronuclear Janus dumbbells (HJD). It has been recently shown that HJD, under appropriate conditions, are able to self-assemble in colloidal micelles [31], promoted by the surface roughness of the particles; they may form colloidal molecules as well as larger supracolloidal structures [32]. In spite of the scientific and technological importance of HJD, few simulation studies have focused on such systems: in particular, an assessment of experimental results in comparison with simulation data has been carried out only in [31, 32]. Therefore, more investigations concerning the phase behaviour of HJD would be highly desirable, in particular to study how the heterogeneity influences the competition between the formation of aggregates and phase separation. From a microscopic viewpoint, such a competition has been generally interpreted in terms of simple spherical models characterized by the simultaneous presence of short-range attractions and long-range repulsions in the total interaction (see e.g. [33–37] and references). Physically, the long-range repulsion generally stems from the weakly screened charge carried by colloidal macromolecules, whereas the short-range attraction stems from several different mechanisms, including depletion forces, van der Waals interactions, hydrophobic effects [38]. In this picture, the formation of clusters out of the homogeneous fluid is interpreted as due to an appropriate balance between attraction, promoting the formation of aggregates at low temperature, and long-range repulsion, preventing a complete phase separation [39, 40]. More recently, the interplay between the aggregate formation and phase separation has been investigated by means of various theoretical and simulation tools also for more sophisticated models, as for instance patchy [41–43] and Janus [44, 45] particles.

In this work HJD are modelled as two tangent hard spheres, with the first one being surrounded by a square-well interaction with fixed attraction range; the heterogeneity is introduced by changing the ratio between the two hard-core diameters. We show by standard Monte Carlo simulations that even moderate asymmetries sensitively influence the overall phase scenario, giving rise to a competition between the gas-liquid phase separation and the spontaneous formation of different self-assembled structures in the fluid. We compare with our previous investigation of homonuclear Janus dumbbells [10] and show that the development of peculiar planar structures (lamellæ) therein observed at low temperatures, is only found around the perfectly symmetric case. At variance, the gas-liquid phase separation, turning to be completely suppressed in the homonuclear case [10], reveals again if the sphere bearing the square-well interaction becomes larger than the second one.

The paper is organized as follows: in Section 2 we detail the interaction properties of the HJD model and the simulation technique we have employed in this study. Results

are reported and discussed in Section 3. Conclusions follow in Section 4.

2. Models and methods

Our dumbbell model is constituted by two tangent hard spheres — characterized by different core diameters σ_1 and σ_2 — with the first one being surrounded by a square-well attraction; the interaction potential among sites i and j ($i, j \in [1, 2]$) on different molecules is then written as:

$$U_{11}(r) = \begin{cases} \infty & \text{if } r < \sigma_1 \\ -\varepsilon & \text{if } \sigma_1 \leq r < \sigma_1 + \lambda\sigma_1 \\ 0 & \text{otherwise} \end{cases} \quad (1a)$$

$$U_{12}(r) = U_{21}(r) = \begin{cases} \infty & \text{if } r < (\sigma_1 + \sigma_2)/2 \\ 0 & \text{otherwise} \end{cases} \quad (1b)$$

$$U_{22}(r) = \begin{cases} \infty & r < \sigma_2 \\ 0 & \text{otherwise} \end{cases} \quad (1c)$$

The diameters σ_1 and σ_2 are defined in terms of a unit of length σ and a parameter α , so that:

$$\begin{cases} \sigma_1 = \alpha\sigma \\ \sigma_2 = \sigma \end{cases} \quad \text{if } 0 < \alpha \leq 1; \quad \begin{cases} \sigma_1 = \sigma \\ \sigma_2 = (2 - \alpha)\sigma \end{cases} \quad \text{if } 1 < \alpha \leq 2 \quad (2)$$

The two limits $\alpha = 0$ and $\alpha = 2$ correspond to pure hard-sphere (HS) and pure square-well (SW) atomic fluids respectively, whereas $\alpha = 1$ is the symmetric case. In the $\alpha = 0$ limit, neither a gas-liquid transition nor the formation of clusters take place whereas, in the $\alpha = 2$ limit, a conventional gas-liquid phase separation (whose critical parameters depend on the width of the attractive square-well) occurs and no cluster formation is expected. Finally, for $\alpha = 1$ we recover the homonuclear Janus dumbbell configuration for which (in the case $\lambda = 0.5$) the gas-liquid phase separation is absent and both spherical and planar (lamellæ) clusters are observed [10]. Models investigated in this work correspond to the size parameter α varying in the range $0.33 \leq \alpha \leq 1.66$ and are schematically depicted in figure 1: the evolution with increasing α from a HS dominating (in size) configuration to the opposite SW dominating one, is therein illustrated. The well depth ε in equation (1a) gives the unit of energy, in terms of which we define the reduced temperature $T^* = k_B T / \varepsilon$ (with k_B as the Boltzmann constant); we also introduce the reduced density $\rho^* = (N/V)\sigma^3$ (where N is the number of particles and V the volume). In all calculations we also set, as in [10], $\lambda = 0.5$ in the definition (1a) of $U_{11}(r)$.

In order to characterize self-assembled structures and thermodynamic properties of HJD, we have carried out standard Monte Carlo simulations of a sample composed by 500 particles enclosed in a cubic box with periodic boundary conditions at four different densities (specifically, $\rho^* = 0.05$, $\rho^* = 0.10$, $\rho^* = 0.20$ and $\rho^* = 0.30$) and several temperatures in the whole investigated range of α -values.

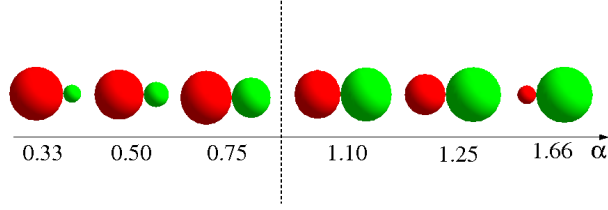


Figure 1. Schematic representation of HJD for all α values investigated in this work, see equation (2). In each pair, left (red) and right (green) spheres correspond to the HS and SW sites, respectively.

We shall make use of the second virial coefficient B_2 , written for a molecular system as [46]:

$$B_2(\beta\epsilon) = -\frac{1}{2} \int f_{ij}(\mathbf{r}) d\mathbf{r} d\Omega_i d\Omega_j \quad (3)$$

where $\beta = 1/T^*$, $f_{ij}(\mathbf{r}) = \exp[-\beta U_{ij}(\mathbf{r})] - 1$ is the Mayer function between molecules i and j and $U_{ij}(\mathbf{r})$ is the intermolecular potential defined by equations (1a)-(1c). Moreover, in equation (3) $\int \dots d\Omega$ represents the integration over all the orientations, normalized so that $\int d\Omega = 1$. Following the method employed by Yethiraj and Hall [47], we have numerically computed B_2 by generating a large number N_c of independent configurations of two dumbbells in a cubic box of side L ; then, by averaging the Mayer function over all such configurations, we obtain:

$$B_2(\beta\epsilon) = -\frac{L^3 \langle f_{ij} \rangle}{2N_c}. \quad (4)$$

Values of $B_2 < 0$ ($B_2 > 0$) indicate that attractive (repulsive) interactions are prevailing, with the Boyle temperature T_B^* , at which $B_2 = 0$, separating the two regimes. In the next section we shall employ T_B^* to locate the regions in the $\alpha - T^*$ plane over which the attractive interactions are more effective.

3. Results and discussion

Using equation (4), we first determine T_B^* as explained in the previous Section. Results as a function of α are reported in figure 2: as visible, the T_B^* vs α locus delimits two regions, over which $B_2 > 0$ and $B_2 < 0$, respectively. In the $B_2 > 0$ region, HJD should not experience enough attractions to give rise to significant particle association. Conversely, in the $B_2 < 0$ region, attractive interactions are effective and clustering or droplet formation may occur; it appears that such a region becomes smaller if α decreases, and disappears in the limit of $\alpha = 0$. In the other limit, in which α approaches 2, i.e. for purely SW spheres, T_B^* gets a saturation value over a limited range of α , thus suggesting the phase behaviour of the ordinary SW fluid to moderately extend inside the $\alpha - T^*$ plane.

We now examine in more detail various heterogeneity regimes.

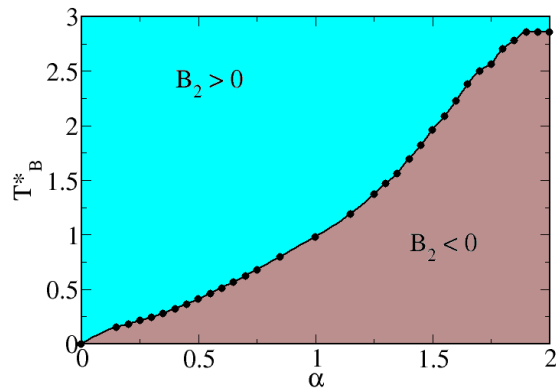


Figure 2. Boyle temperature T_B^* (circles, with the line as a guide to the eye) vs α . The upper (cyan) and lower (brown) regions correspond, respectively, to positive and negative values of the second virial coefficient B_2 .

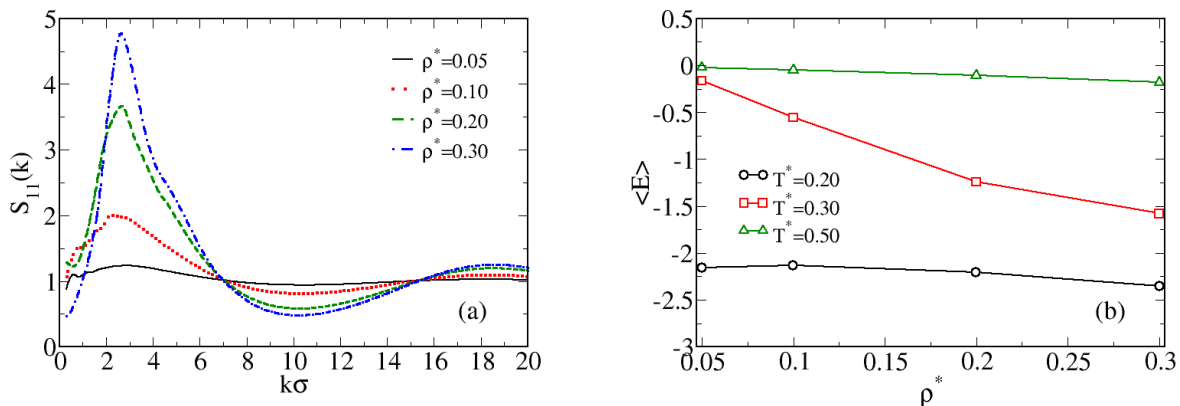


Figure 3. Panel (a): $S_{11}(k)$ for $\alpha = 0.33$ at $T^* = 0.30$ and several densities. Panel (b): average internal energy per particle $\langle E \rangle$ vs ρ^* along different isotherms.

3.1. Cluster formation ($0.33 < \alpha < 1$)

We recall that for $\alpha < 1$ the attractive (SW) sphere is smaller than the repulsive (HS) one. We first consider $\alpha = 0.33$. The SW-SW structure factors $S_{11}(k)$ are shown in figure 3a at $T^* = 0.30$ (i.e. slightly above T_B^* according to figure 2), and for various densities. All $S_{11}(k)$ show a low- k peak, becoming more pronounced as the density increases, whereas $S_{11}(k \rightarrow 0)$ remain limited, such a behaviour appearing compatible with the formation of a cluster fluid that suppresses the gas-liquid phase separation (see also [48]). Indeed, both experiments [48, 49] and theoretical studies (see e.g. [33–35] and references) point to such a low- k peak as indicating the formation of aggregates. More generally, the presence of the low- k peak has been recently related to the onset of some

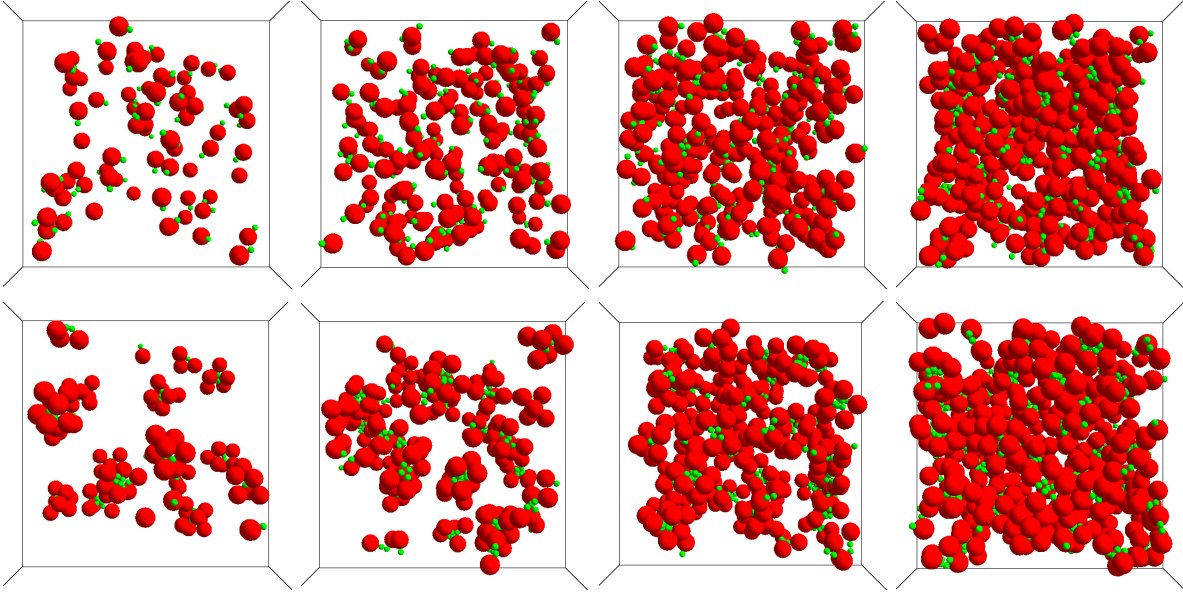


Figure 4. Typical microscopic configurations with $\alpha = 0.33$ at $T^* = 0.30$ (top panels) and $T^* = 0.20$ (bottom panels) and increasing densities (from left to right, $\rho^* = 0.05$, 0.10 , 0.20 and 0.30).

kind of “intermediate-range order” in the fluid [37, 50, 51].

The formation of the cluster fluid can be further investigated by monitoring the average internal energy per particle $\langle E \rangle$ (in units of ε) over an extended temperature range encompassing T_B^* : as visible from figure 3b, the almost flat behaviour of $\langle E \rangle$ vs ρ^* at $T^* = 0.50$ is replaced by a monotonic decay at $T^* = 0.30$, becoming flat again at $T^* = 0.20$. These outcomes indicate that, at the highest temperature, clusters are not able to develop, since $\langle E \rangle \approx 0$ regardless of the density. At $T^* = 0.30$, instead, the attractive energy is strong enough to drive a cluster assembly process, provided the density is high enough, as signalled by the strong enhancement of the low- k peak of $S_{11}(k)$, occurring only for $\rho^* \geq 0.2$ (see figure 3a). Finally, if the temperature is further lowered down to $T^* = 0.20$, the system is able to assemble into clusters even at low density; indeed, at this temperature, the energy attains almost the same (significantly negative) value, irrespective of the density. Typical microscopic configurations at $T^* = 0.30$ and 0.20 , displayed in figure 4, confirm the above picture; note in particular that at $T^* = 0.20$ (bottom panels) clusters are visible even in the low density regime. It is worth noting that, under appropriate conditions for the development of clusters, the ratio $|\langle E \rangle|/T^*$ ranges approximately between 3 and 10, thus confirming the relative stability of aggregates; on the other hand, this does not preclude the possibility for particles to rearrange within the clusters, as well as to be exchanged between clusters and the surrounding medium, as also observed in experiments [31]). Our analysis is further supported by the probability distribution of bonds, $P(N_b)$ shown in figure 5 — where N_b is the number of bonds per particle, assuming two particles as bonded together if the distance between the SW spheres falls within the corresponding attraction range,

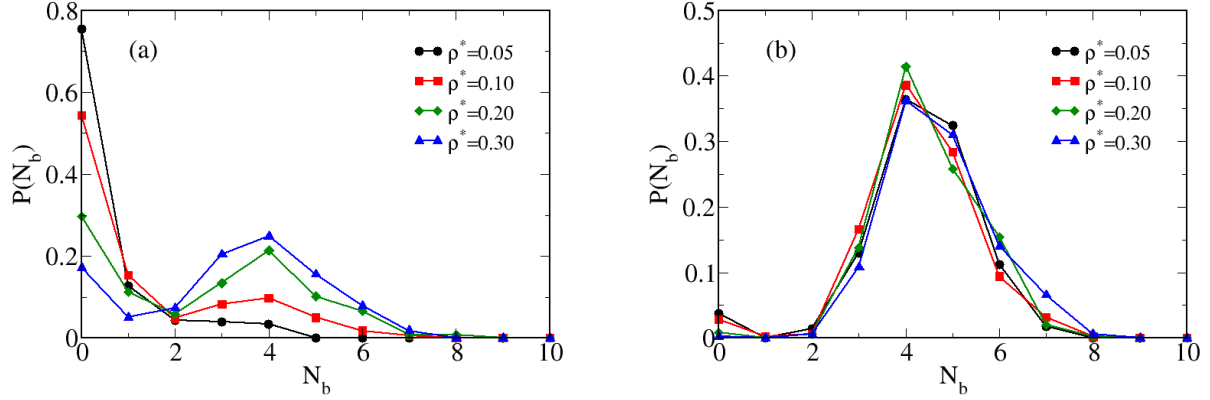


Figure 5. Probability distribution of bonds with $\alpha = 0.33$ for several densities at (a) $T^* = 0.30$ and (b) $T^* = 0.20$. Lines are guides to the eye.

i.e. between σ_1 and $\sigma_1 + \lambda\sigma_1$. One can notice that at $T^* = 0.30$ (panel a), a maximum value is attained for $N_b = 0$ at $\rho^* = 0.05$, this suggesting that few bonds among HJD are formed in such conditions. The maximum shifts towards higher values of N_b only upon increasing ρ^* . Things drastically change when $T^* = 0.20 < T_B^*$ (panel b), with the maximum of $P(N_b)$ centred around $N_b = 4$ and almost insensitive to density variations. Note that the value attained by the internal energy $|\langle E \rangle| \approx 2$ when $T^* = 0.20$ (see figure 5b) is congruent with a bond configuration in which each dumbbell forms four bonds, since $|\langle E \rangle|$ scales with $N_b/2$. We have observed that at $T^* = 0.20$ and for the various densities examined in this work, clusters are formed by three to ten particles. In such conditions, we have preliminarily calculated the average radius of gyration of clusters $\langle R_g \rangle$, as function of their size. We have found that specific values of $\langle R_g \rangle$ attained for a given cluster size do not practically depend on the density of the system. In general, the trend observed for $\langle R_g \rangle$ as a function of the cluster size, along with visual inspection of cluster configurations (see especially bottom panels of figure 4), suggests that roughly spherical aggregates develop in the system.

Upon increasing α , but still keeping below $\alpha = 1$, T_B^* increases (see figure 2) and HJD can bond together already at higher T^* . However, the structural properties do not change qualitatively: $S_{11}(k)$ still display a low- k peak whereas $S_{11}(k \rightarrow 0)$ remain limited, as shown in figure 6 where results concerning $\alpha = 0.5$ and $\alpha = 0.75$ at $T^* = 0.30$ are reported. Some new features emerge in the probability distribution of bonds, as a consequence of the larger number of HJD that can assemble into a cluster: specifically, $P(N_b)$, reported in figure 7, now displays multiple peaks at high densities indicating an increased inhomogeneity in the dumbbell bonding environments. Such features appear compatible with two distinct components of the clusters, namely capping dumbbells, constituting either the total surface of the aggregate or caps of elongated structures (associated to the first peak), and bulk dumbbells (associated to the second peak). At

low densities, when smaller clusters are favoured, only the first configuration occurs. When the average cluster size becomes larger than ≈ 10 , both capping and bulk arrangements are observed yielding an additional peak. A more detailed analysis of

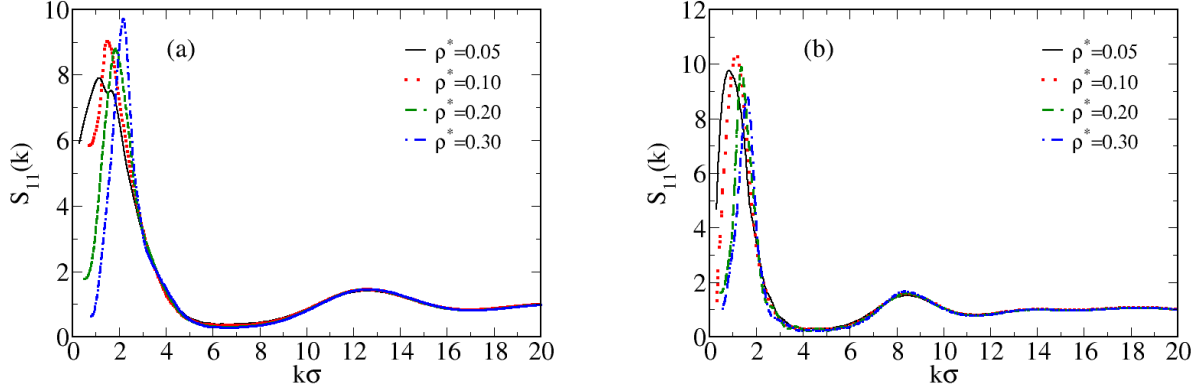


Figure 6. $S_{11}(k)$ at $T^* = 0.30$ and several densities with (a) $\alpha = 0.50$ and (b) $\alpha = 0.75$.

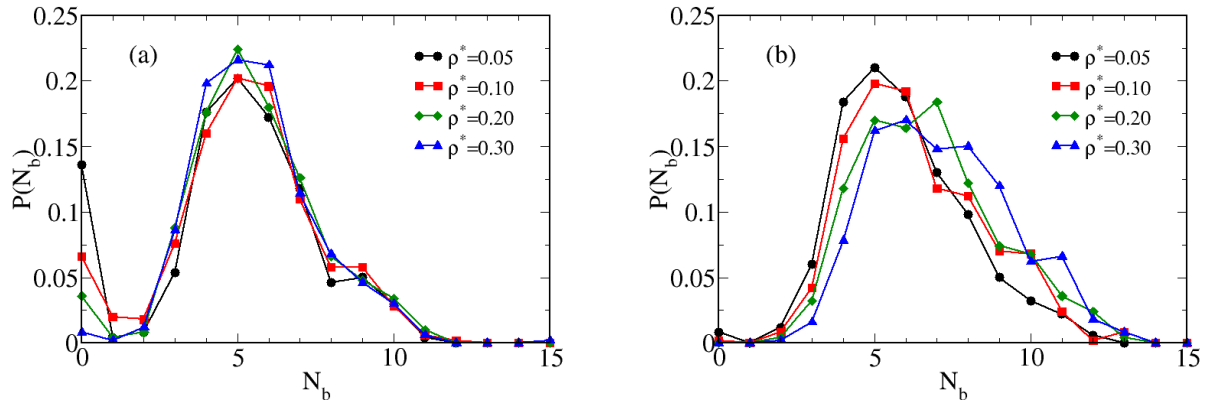


Figure 7. Probability distribution of bonds at $T^* = 0.30$ and several densities with (a) $\alpha = 0.50$ and (b) $\alpha = 0.75$. Lines are guides to the eye.



Figure 8. Sketch of a cluster composed by ten HJD molecules with $\alpha = 0.75$ at $T^* = 0.30$, as obtained by MC simulations.

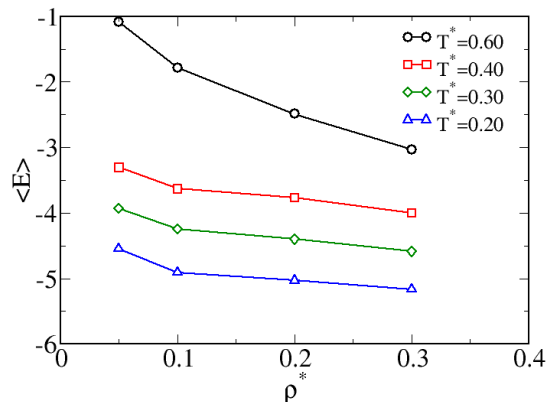


Figure 9. Average internal energy per particle $\langle E \rangle$ with $\alpha = 1.10$ as a function of the density along different isotherms.

particle distribution inside the cluster seems in order to better resolve this possibility.

Interestingly enough, the above findings qualitatively agree with experimental results [31] on self-assembly of dumbbell-shaped particles in colloidal micelles. Here, results are presented concerning synthesized dumbbell particles with one rough (“hard-sphere”) and one smooth (“square-well”) sphere, interacting through depletion interactions. As the size ratio between smooth and rough sphere falls around (1.11/1.46) micron, particles self-assemble into colloidal micelles, a result in close correspondence with our observations in the same conditions (i.e. with $\alpha \sim 0.75$), as documented for instance by the snapshot taken from our MC simulation reported in figure 8.

3.2. Competition between cluster formation and phase separation ($\alpha = 1.10$)

As we have shown in Ref. [10] no gas-liquid coexistence takes place at $\alpha = 1$, and results from Section 3.1 indicate that this holds for all $\alpha < 1$. Such a scenario changes remarkably as soon as α gets larger than unity. We first consider results for $\langle E \rangle$ at $\alpha = 1.10$, reported in figure 9: the monotonic decrease of the energy with increasing density, visible at high temperatures, is progressively replaced by an almost flat trend as the temperature goes down to $T^* = 0.2$, where the internal energy is almost constant for all ρ^* . The absence of jumps in $\langle E \rangle$ suggests that no large-scale aggregates (as, for instance, lamellæ) are formed in the system. On the other hand, $S_{11}(k)$ at $T^* = 0.60$ (shown in figure 10a) clearly displays a low- k peak for all densities, this feature suggesting the development of clusters in the system. Conversely, if the temperature is lowered to $T^* = 0.20$ (figure 10b), the low- k peak disappears at low and intermediate densities and survives only at $\rho^* = 0.30$; the disappearance of the low- k peak gives place to the rise of the $k \rightarrow 0$ limit of $S_{11}(k)$, suggesting that a phase separation process is taking place.

Such observations are compatible with a competition between self-assembly

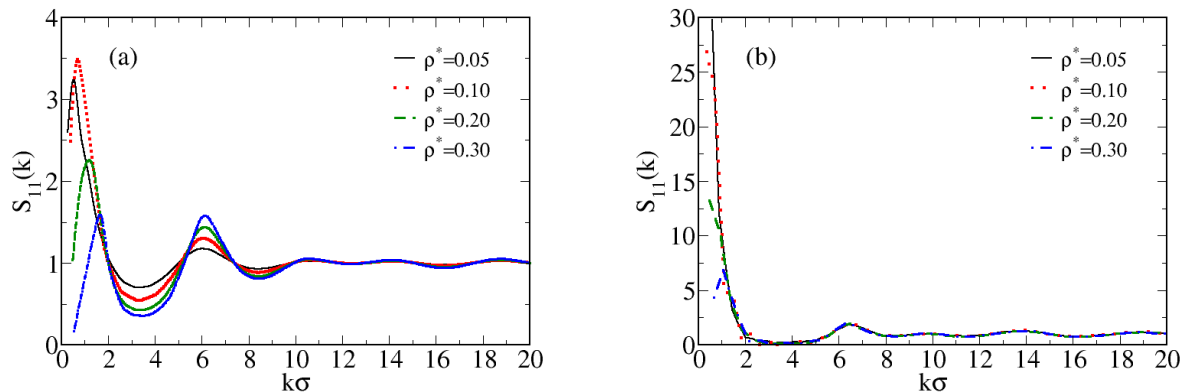


Figure 10. $S_{11}(k)$ with $\alpha = 1.10$ and for several densities at (a) $T^* = 0.60$, and (b) $T^* = 0.20$.

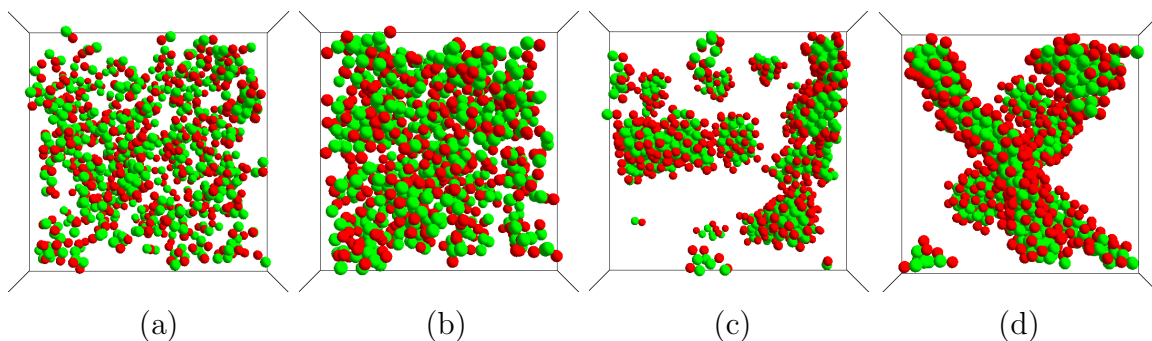


Figure 11. Typical microscopic configurations with $\alpha = 1.10$ at $T^* = 0.60$ (a, b) and 0.20 (c, d) and $\rho^* = 0.05$ (a, c), and 0.10 (b, d).

processes (at high temperature) and gas-liquid phase coexistence (at lower temperatures). Note, in this instance, that here, unlike previous cases, both $T^* = 0.60$ and $T^* = 0.20$ are lower than T_B^* (see figure 2), this indicating that the competition between the two regimes occur when the attractive part of the interaction is significant. Visual evidence is offered by snapshots of microscopic configurations displayed in figure 11: HJD assemble in small clusters at $T^* = 0.60$ and densities $\rho^* = 0.05$ and $\rho^* = 0.10$ (first two panels); upon lowering the temperature, the phase separation process dominates, as visible in the last two panels corresponding to $T^* = 0.20$ and $\rho^* = 0.05$ and $\rho^* = 0.10$.

3.3. Phase separation ($1.25 \leq \alpha \leq 1.66$)

In this regime the SW interaction becomes significantly larger than the HS one. The ensuing reduced role of short-range repulsion should favour the phase separation mechanism. We illustrate this point through simulations carried out at $\alpha = 1.25$ and

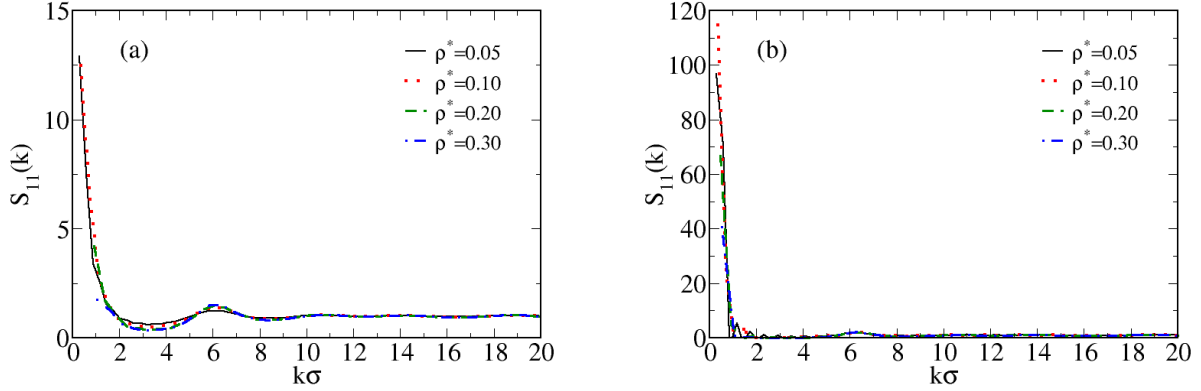


Figure 12. $S_{11}(k)$ at $T^* = 0.60$ and for several densities with (a) $\alpha = 1.25$ and (b) $\alpha = 1.66$.

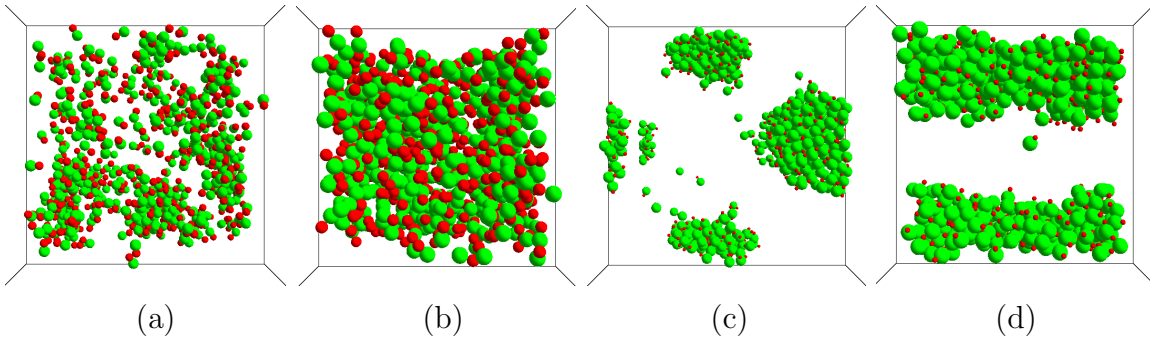


Figure 13. Typical microscopic configurations at $T^* = 0.60$ with $\alpha = 1.25$ (a, b) and $\alpha = 1.66$ (c, d) and $\rho^* = 0.05$ (a, c) and $\rho^* = 0.20$ (b, d).

$\alpha = 1.66$, for $T^* = 0.60$ (i.e. below T_B^* , see figure 2) and increasing densities. All $S_{11}(k)$, reported in figure 12, show a clear diverging trend with $k \rightarrow 0$, thus indicating that the system is close to (or has already crossed) a metastable region. This observation is supported by snapshots reported in figure 13, where no clusters are observed, either at high or low density; the phase-separation process is instead clearly visible in panels (c) and (d), where the system appears separated into gas and liquid regions.

The generic phase behaviour of HJD is schematically reported in table 1, where the presence (or absence) of clusters, lamellæ and phase separation is recorded as a function of α . Such different arrangements are also displayed in figure 14, concerning specifically the thermodynamic condition $T^* = 0.30$ and $\rho^* = 0.10$. To summarize, the competition between cluster formation and phase separation favours the former at low/intermediate values of α and the latter at intermediate/high values of α . Accordingly, one can reasonably surmise that the presence of both is possible only over an intermediate narrow interval, namely for α between 1.00 and 1.10. As a consequence, a subtle equilibrium exists between phase separation and self-assembly, strongly depending upon

Table 1. Phase behaviour of HJD as a function of α . Corresponding values of the HS (σ_1) and SW (σ_2) diameters are indicated. Note that if $\alpha = 0$ the model reduces to a single hard-sphere particle and, at the opposite end, to a single square-well particle.

α	σ_1	σ_2	Clusters	Lamellae	Phase Separation
0.00	0.00	1.00	✗	✗	✗
0.33	0.33	1.00	✓	✗	✗
0.50	0.50	1.00	✓	✗	✗
0.75	0.75	1.00	✓	✗	✗
1.00	1.00	1.00	✓	✓	✗
1.10	1.00	0.90	✓	✗	✓
1.25	1.00	0.75	✗	✗	✓
1.50	1.00	0.50	✗	✗	✓
1.66	1.00	0.34	✗	✗	✓
2.00	1.00	0.00	✗	✗	✓

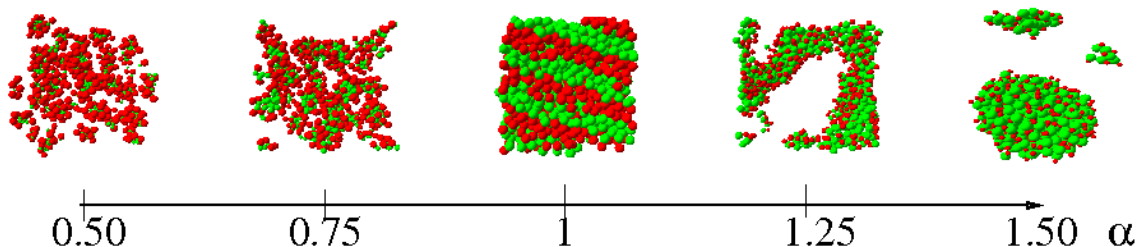


Figure 14. Phase behaviour of HJD as a function of α (at fixed $T^* = 0.30$ and $\rho^* = 0.10$). As visible, the planar configuration (lamellae) is observed only around the homonuclear case ($\alpha = 1$).

the heterogeneity of HJD. Lamellar structures are hardly observed upon varying α , this suggesting that only $\alpha \approx 1$ is compatible with the development of lamellae, as found in our previous work [10]. There, the simultaneous presence of both clusters and lamellae has been documented by the behaviour of an order parameter quantifying the average relative orientations of dimers, and the rotational invariant of local bond order parameters q_6 . It is worth noting that it does not exist a value of α compatible with the simultaneous presence of clusters, lamellae and phase separation; instead, as documented in [10], this may happen in specific cases for homonuclear square-well dumbbells.

4. Conclusions

We have investigated the self-assembly process and gas-liquid phase separation taking place in heteronuclear Janus dumbbells (HJD), modelled by two tangent hard spheres with different core diameters, the first one being surrounded by a square-well attraction. We have carried out standard Monte Carlo simulations to characterize the fluid

structure, the distribution of bonds among molecules, and to study the formation of clusters and phase separations.

The relative size of the two spheres constituting one HJD molecule has been changed by introducing a parameter α : for $\alpha < 1$ (corresponding to the square-well site smaller than the hard-sphere one), we have observed the development of a cluster phase, with spherical aggregates becoming increasingly structured upon lowering the temperature. Here, no indication emerges on the presence of a gas-liquid critical behaviour, thus suggesting that the cluster formation suppresses the phase separation. These findings qualitatively agree with experimental results cataloguing the self-assembly of dumbbell-shaped particles [31]. Moving towards $\alpha = 1$, the square-well attraction increases, allowing for a progressively large number of bonds per molecule to be established; as a consequence, HJD may self-assemble into relatively large clusters of different sizes and shapes. In the case $\alpha = 1$, corresponding to homonuclear Janus dumbbells, we have previously documented [10] the absence of a gas-liquid coexistence and the simultaneous appearance of planar structures (lamellae). The development of these latter turns to depend sensitively on the symmetry of dumbbells, and therefore is essentially confined to the homonuclear case. Finally, if α is further increased, the attractive interaction becomes more and more isotropic and the gas-liquid phase separation progressively dominates, first competing with (till $\alpha = 1.10$), then completely suppressing the formation of clusters.

Our model may constitute a useful prototype to investigate the role of size asymmetry and attractive interactions in the phase behaviour of dumbbell-shaped colloids with different chemical compositions, allowing for a deeper understanding of the competition between self-assembly and phase separation in such systems.

Acknowledgements

GM, DC, CC, FS and AG gratefully acknowledge support from PRIN-MIUR 2010-2011 project. AG, PO'T and TSH acknowledge support of a Cooperlink bilateral agreement Italy-Australia.

References

- [1] Nagao D, Goto K, Ishii H and Konno M 2011 *Langmuir* **27** 13302
- [2] Rozynek Z, Mikkelsen A, Dommersnes P and Fossum J O 2014 *Nat. Comm.* **5** 3945
- [3] Riley E K and Watson C M L 2014 *J. Appl. Phys.* **115** 223514
- [4] Yoon K, Lee D, Kim J W, Kim J and Weitz D A 2012 *Chem. Comm.* **48** 9056
- [5] Forster J D, Park J G, Mittal M, Noh H, Schreck C F, O'Hern C S, Cao H, Furst E M and Dufresne E R 2011 *ACS Nano* **5** 6695
- [6] Ma F, Wang S, Smith L and Wu N 2012 *Advanced Functional Materials* **22** 4334
- [7] Hosein I D and Liddell C M 2007 *Langmuir* **23** 10479

- [8] Fejer S N, Chakrabarti D, Kusumaatmaja H and Wales D J 2014 *Nanoscale* **6** 9448
- [9] Munaò G, Costa D, Giacometti A, Caccamo C and Sciortino F 2013 *Phys. Chem. Chem. Phys.* **15** 20590
- [10] Munaò G, O’Toole P, Hudson T S, Costa D, Caccamo C, Giacometti A and Sciortino F 2014 *Soft Matter* **10** 5269
- [11] Milinkovic K, Dennison M and Dijkstra M 2013 *Phys. Rev. E* **87** 032128
- [12] Munaò G, Costa D and Caccamo C 2009 *Chem. Phys. Lett.* **470** 240
- [13] Munaò G, Costa D and Caccamo C 2009 *J. Chem. Phys.* **130** 144504
- [14] Marechal M and Dijkstra M 2008 *Phys. Rev. E* **77** 061405
- [15] Ni R and Dijkstra M 2011 *J. Chem. Phys.* **134** 034501
- [16] Marechal M, Goetzke H H, Härtel A and Löwen H 2011 *J. Chem. Phys.* **135** 234510
- [17] Dennison M, Milinkovic K and Dijkstra M 2012 *J. Chem. Phys.* **137** 044507
- [18] Chapela G A, de Rio F and Alejandre J 2011 *J. Chem. Phys.* **134** 224105
- [19] Miller M A, Blaak R, Lumb C N and Hansen J P 2009 *J. Chem. Phys.* **130** 114507
- [20] Ilg P and Gado E D 2011 *Soft Matter* **7** 163
- [21] Chong S H, Moreno A J, Sciortino F and Kob W 2005 *Phys. Rev. Lett.* **94** 215701
- [22] Tu F, Park B J and Lee D 2013 *Langmuir* **29** 12679
- [23] Park B J and Lee D 2012 *Acs Nano* **6** 782
- [24] Jackson A M, Myerson J W and Stellacci F 2004 *Nat. Mat.* **3** 330–336
- [25] Roh K H, Martin D C and Lahann J 2005 *Nat. Mat.* **4** 759–763
- [26] Wang B, Li B, Zhao B and Li C Y 2008 *J. Am. Chem. Soc.* **130** 11594–11595
- [27] Hong L, Cacciuto A, Luijten E and Granick S 2008 *Langmuir* **24** 621–625
- [28] Chen C H, Shah R K, Abate A R and Weitz D A 2009 *Langmuir* **25** 4320–4323
- [29] Jiang B S, Chen Q, Tripathy M, Luijten E, Schweizer K and Granick S 2010 *Advanced Materials* **22** 1060
- [30] Chen Q, Whitmer J K, Jiang S, Bae S C, Luijten E and Granick S 2011 *Science* **331** 199
- [31] Kraft D J, Ni R, Smalenburg F, Hermes M, Yoon K, Weitz D, van Blaaderen A, Groenewold J, Dijkstra M and Kegel W 2012 *PNAS* **109** 10787
- [32] Skelhon T S, Chen Y and Bon S A F 2014 *Soft Matter* **10** 7730
- [33] Cardinaux F, Stradner A, Schurtenberger P, Sciortino F and Zaccarelli E 2007 *Europhys. Lett.* **77** 48004
- [34] J M Bomont and J L Bretonnet and D Costa 2010 *J. Chem. Phys.* **132** 084506
- [35] Bomont J M and Costa D 2012 *J. Chem. Phys.* **137** 164901
- [36] Godfrin P D, Castañeda-Priego R, Liu Y and Wagner N J 2013 *J. Chem. Phys.* **139** 154904

- [37] Godfrin P D, Valadez-Pérez N E, Castañeda-Priego R, Wagner N J and Liu Y 2014 *Soft Matter* **10** 5061
- [38] Russel W B, Saville D A and Schowalter W R 1991 *Colloidal Dispersions* (Cambridge University Press)
- [39] Pini D, Jialin G, Parola A and Reatto L 2000 *Chem. Phys. Lett.* **327** 209
- [40] Imperio A and Reatto L 2004 *J. Phys.: Condens. Matter* **16** S3769
- [41] Reinhardt A, Williamson A J, Doye J P K, Carrete J, Varela L M and Louis A A 2011 *J. Chem. Phys.* **134** 104905
- [42] Russo J, Tavares J M, Teixeira P, da Gama M M T and Sciortino F 2011 *Phys. Rev. Lett.* **106** 085703
- [43] Rovigatti L, Tavares J M and Sciortino F 2013 *Phys. Rev. Lett.* **111** 168302
- [44] Sciortino F, Giacometti A and Pastore G 2009 *Phys. Rev. Lett.* **103** 237801
- [45] Sciortino F, Giacometti A and Pastore G 2010 *Phys. Chem. Chem. Phys.* **12** 11869
- [46] Hansen J P and McDonald I R 2006 *Theory of simple liquids*, 3rd Ed. (Academic Press, New York)
- [47] Yethiraj A and Hall C K 1991 *Mol. Phys.* **72** 619
- [48] Stradner A, Sedgwick H, Cardinaux F, Poon W C K, Egelhaaf S U and Schurtenberger P 2004 *Nature* **432** 492
- [49] Liu Y, Fratini E, Baglioni P, Chen W R and Chen S H 2005 *Phys. Rev. Lett.* **95** 118102
- [50] Liu Y, Porcar L, Chen J, and Baglioni P 2011 *J. Phys. Chem. B* **115** 7238
- [51] Falus P, Porcar L, Fratini E, Chen W R, Faraone A, Hong K, Baglioni P and Liu Y 2012 *J. Phys.: Condens. Matter* **24** 064114